

The impact of dust on sulfate aerosol, CN and CCN during an East Asian dust storm

P. T. Manktelow, K. S. Carslaw, G. W. Mann, and D. V. Spracklen

School of Earth and Environment, University of Leeds, Leeds, UK

Received: 4 June 2009 – Published in Atmos. Chem. Phys. Discuss.: 8 July 2009

Revised: 11 December 2009 – Accepted: 5 January 2010 – Published: 18 January 2010

Abstract. A global model of aerosol microphysics is used to simulate a large East Asian dust storm during the ACE-Asia experiment. We use the model together with size resolved measurements of aerosol number concentration and composition to examine how dust modified the production of sulfate aerosol and the particle size distribution in East Asian outflow. Simulated size distributions and mass concentrations of dust, sub- and super-micron sulfate agree well with observations from the C-130 aircraft. Modeled mass concentrations of fine sulfate ($D_p < 1.3 \mu\text{m}$) decrease by $\sim 10\%$ due to uptake of sulfur species onto super-micron dust. We estimate that dust enhanced the mass concentration of coarse sulfate ($D_p > 1.0 \mu\text{m}$) by more than an order of magnitude, but total sulfate concentrations increase by less than 2% because decreases in fine sulfate have a compensating effect. Our analysis shows that the sulfate associated with dust can be explained largely by the uptake of H_2SO_4 rather than reaction of SO_2 on the dust surface, which we assume is suppressed once the particles are coated in sulfate. We suggest that many previous model investigations significantly overestimated SO_2 oxidation on East Asian dust, possibly due to the neglect of surface saturation effects. We extend previous model experiments by examining how dust modified existing particle concentrations in Asian outflow. Total particle concentrations (condensation nuclei, CN) modeled in the dust-pollution plume are reduced by up to 20%, but we predict that dust led to less than 10% depletion in particles large enough to act as cloud condensation nuclei (CCN). Our analysis suggests that E. Asian dust storms have only a minor impact on sulfate particles present at climate-relevant sizes.

1 Introduction

The Gobi (China/Mongolia) and Taklimakan (China) deserts are the most important sources of dust in E. Asia. During springtime, the combined effect of strong winds, low rainfall and sparse vegetation cover leads to the generation of large quantities of dust, which can be transported as far east as N. America (e.g., Van Curen and Cahill, 2002; Zhao et al., 2008). During transport, the dust can become internally mixed with other chemical species through condensation, coagulation, surface chemical reactions, and aqueous phase chemical reactions in cloud drops containing dust (cloud processing). Observations show that secondary aerosol species such as sulfate and nitrate often exist as surface coatings on Asian dust as a result of these processes (Mori et al., 2003; Ooki and Uematsu, 2005; Perry et al., 2004; Tang et al., 2004a, b; Trochkin et al., 2003; Xiao et al., 1997; Zhang et al., 2000; Sullivan et al., 2007; Matsuki et al., 2005a, b). The presence of this material can enhance the solubility of dust particles, increasing their ability to act as cloud drop or ice immersion nuclei (Perry et al., 2004), and can increase the bioavailability of iron, which enhances the fertilisation of marine phytoplankton (Jickells et al., 2005; Meskhidze et al., 2003, 2005). A further consequence of the uptake of secondary aerosol material, considered in this study, is that existing aerosol could be affected by dust via reduced concentrations of aerosol precursor gases, thereby influencing existing particle concentrations and even cloud condensation nuclei by reduced growth and new particle formation.

Heterogeneous reactions between acidic gases (e.g., SO_2 , H_2SO_4 , HNO_3) and dust have been examined extensively in the laboratory (Adams et al., 2005; Goodman et al., 2001; Li et al., 2006; Ullerstam et al., 2002, 2003; Usher et al., 2002; Prince et al., 2007), but the mechanism and rate at which inorganic ions form on dust remain uncertain. In this study



Correspondence to: K. S. Carslaw
(k.s.carslaw@leeds.ac.uk)

we are interested in sulfate formation on mineral dust. Knudsen cell reactors measure an initial uptake coefficient for SO_2 that varies by several orders of magnitude (10^{-4} (Goodman et al., 2001)– 10^{-7} (Usher et al., 2002), BET surface area) depending on the morphology, surface area and composition of dust. Goodman et al. (2001) showed that dust surfaces lose their reactivity with SO_2 at a surface molecular coverage of approximately 10^{14} cm^{-2} , although there is evidence that further reactions can occur at high humidity (Ullerstam et al., 2002; Prince et al., 2007).

Several models have been used to examine dust-sulfur interactions, but a lack of knowledge on the chemical composition of dust derived from different source regions leads to a large range in the SO_2 uptake coefficient implemented in models. Few models consider surface saturation effects once sulfate begins to form on the dust surface. Instead, some assume that ozone controls the amount of SO_2 oxidized on dust and limit the reaction according to the dust alkalinity (Dentener et al., 1996; Liao et al., 2003). The range of SO_2 uptake coefficients observed for different mineral components and assumptions about the reactivity of dust translate into a large range in modeled reaction rates. Several model studies estimate that the presence of dust increases sulfate mass concentrations by a factor of 2 across E. Asia because of the extra reactive surface for SO_2 oxidation to sulfate (Dentener et al., 1996; Bauer et al., 2005) while other studies calculate less than a 5% enhancement (Liu et al., 2005; Pozzoli et al., 2008).

Observations of the chemical composition of dust can help evaluate and constrain the reaction rates used in models. The reactive constituents of dust particles in East Asia are CaCO_3 , MgCO_3 , and $\text{CaMg}(\text{CO}_3)_2$. The balance between CO_3^{2-} and Ca/Mg chemical equivalences provides an indication of the chemical age of dust, since CO_3^{2-} is displaced by NO_3^- and SO_4^{2-} during chemical aging (Song and Carmichael, 2001b; Tang et al., 2004b; Song et al., 2007). Song et al. (2007) analyzed the composition of fine dust particles sampled in the ACE-Asia experiment and found that a large fraction of CO_3^{2-} remained in E. Asian dust relative to Ca/Mg, even when the particles had a long contact time (~ 2 d) with acidic gases. They used a Lagrangian photochemical box model to show that the CO_3^{2-} fraction could be reproduced only if the rate of sulfate and nitrate formation on dust was significantly slower than in previous models.

The impact of dust on the particle size distribution is very poorly constrained, but potentially important for climate. Aside from the obvious direct radiative forcing due to the dust itself, the dust may have indirect effects on the existing particle size distribution. Dust can coagulation scavenge small nuclei, and uptake of H_2SO_4 vapor and its precursor SO_2 on dust may suppress new sulfate particle formation, and reduce growth by condensation and cloud processing. These effects would reduce total condensation nuclei (CN) and cloud condensation nuclei (CCN) concentrations,

although the effect on CCN may be partly compensated or reversed by additional CCN from dust particles internally mixed with soluble material. Lee et al. (2009) studied dust impacts on global CCN using the GISS-TOMAS global microphysical model and found that total CCN over dust source regions either doubled or decreased by as much as 20% depending on the size distribution of dust emissions. However, they did not consider heterogeneous oxidation of SO_2 on dust and did not examine how these interactions specifically modified the production and size distribution of sulfate.

The presence of dust would be expected to redistribute sulfate to the larger particles. Clarke et al. (2004) observed that the refractory volume ratio of accumulation mode (volatile + refractory) aerosol increased during dust events in ACE-Asia. They argued that this was the result of volatiles condensing upon coarse dust rather than particles in the accumulation mode, causing an increase in the fraction of refractory species present at sub-micrometer sizes. Howell et al. (2006) later used aerosol optical measurements from ACE-Asia to show that the repartitioning of volatile species to larger, less optically active particle sizes reduced the mass scattering efficiency of secondary aerosol components by as much as 50%.

Few model studies have examined the impact of dust on the size distribution of sulfate particles. Song and Carmichael (2001) separated modeled aerosol mass concentrations into sub and super-micron size classes when calculating gas-particle interactions, and simulated super-micron sulfate fractions of 30–70% across E. Asia as a result of surface reactions on super-micron dust. Tang et al. (2004b) simulated aerosol mass concentrations in 4 size sections, and estimated that 10–30% of sulfate mass existed at super-micron sizes during a significant dust storm in the ACE-Asia campaign. The uptake of acidic gases onto dust is a diffusion-reactive process, which means that the size distribution of dust-associated sulfate will be governed partly by the surface area distribution of dust. Neither study evaluated or based modeled dust size distributions on observations of E. Asian dust, which adds a large degree of uncertainty to the size distribution modeled for dust-associated sulfate.

In this paper, we use the Global Model of Aerosol Processes with bin-resolved microphysics (GLOMAP-bin) to examine dust-sulfate interactions in the ACE-Asia campaign. GLOMAP-bin allows the impacts of dust on the sulfate size distribution to be simulated in more detail than previous models used to examine the ACE-Asia campaign (e.g., Tang et al., 2004a, b). Size resolved measurements of aerosol particle concentration and composition were obtained during a significant dust event (6–15 April) on several NCAR C-130 flights over the Yellow Sea. Using these data we tune our model to reproduce the dust size distribution observed during the dust storm. We then examine dust impacts on sub and super-micron sulfate mass concentrations, and evaluate our results against size-resolved measurements of sulfate mass obtained from the C-130 aircraft. Finally, we extend

previous studies by examining how the dust storm modified the CN and CCN number concentrations observed.

2 Model description

GLOMAP is an extension to the TOMCAT offline 3-D chemical transport model (Chipperfield, 2006). The aerosol size distribution is treated using either a sectional (GLOMAP-bin; Spracklen et al., 2005a, b) or modal scheme (GLOMAP-mode; Manktelow et al., 2007).

2.1 The GLOMAP-bin model

A detailed description of GLOMAP-bin is given in Spracklen et al. (2005a). We use a horizontal resolution of $2.8^\circ \times 2.8^\circ$ with 31 hybrid σ - p levels extending from the surface to 10 hPa. Large scale atmospheric transport and meteorology are specified from European Centre for Medium-Range Weather Forecasts (ECMWF) analyses at 6-hourly intervals. The aerosol processes simulated in the model are: binary homogeneous nucleation of H_2SO_4 and H_2O (Kulmala et al., 1998), condensation of H_2SO_4 , heterogeneous oxidation of SO_2 on dust, hygroscopic growth, coagulation, wet and dry deposition, transport, and cloud processing (SO_2 oxidation by H_2O_2).

The simulations include 2 particle size distributions and 7 aerosol components. The first distribution has 12 size bins, with bin centers geometrically spaced (constant mass ratio) from 200 nm to $40 \mu\text{m}$ dry diameter. This distribution includes only fresh dust, which is assumed to be insoluble and therefore does not form cloud drops (although it is impaction scavenged by rain). The second distribution has 20 size bins between 5 nm and $40 \mu\text{m}$ dry diameter. This distribution is partly soluble and includes sulfate, sea-salt, black carbon (BC), organic carbon (OC) and dust that has aged through interactions with sulfur species. The mass of each component and the number of particles in each bin are tracked. Fresh dust particles are transferred to the soluble distribution after they have aged through the condensation of H_2SO_4 , heterogeneous oxidation of SO_2 (to form surface SO_4), or coagulation with soluble aerosol. The ageing rate is determined by the number of molecules of sulfate on the dust particle surface and it is assumed that a mono-molecular layer is required to transfer dust to the soluble distribution.

Concentrations of the oxidants OH, NO_3 , H_2O_2 , HO_2 and O_3 are interpolated temporally using 6-hourly monthly mean 3-D concentrations from TOMCAT simulations with a comprehensive tropospheric chemistry scheme. Aqueous phase oxidation of SO_2 in cloud drops is assumed to occur only in low clouds, which are specified from monthly mean International Satellite Cloud Climatology Project (ISCCP) data. We assume that all soluble particles larger than 50 nm dry diameter are activated into droplets. We have previously tested a range of size assumptions to account for variability

in updraught speeds and feedback of the aerosol on cloud supersaturation, but the effect on the aerosol size distribution was found to be small (Spracklen et al., 2007).

The model advection timestep is 30 min; emissions, chemistry and microphysical processes are calculated with a timestep of 15 min, and nucleation/condensation with 3 min. Changing the length of the timestep was found to change GLOMAP-bin total aerosol number concentrations by less than 5% (Spracklen et al., 2005b).

2.2 Emissions

Modeled sulfur emissions include SO_2 from anthropogenic (Cofala et al., 2005), biomass burning (Van der Werf et al., 2003), and volcanic (Andres and Kasgnoc, 1998; Halmer et al., 2002) sources. Volcanic SO_2 emissions from Mt. Oyama (Miyakejima island), Japan are also included here, accounting for 27.4 Gg d^{-1} of SO_2 (Satake et al., 2004; Uno et al., 2003). We assume that 2.5% of SO_2 from these continental sources is emitted as primary sulfate particles at particle sizes recommended by Stier et al. (2005). DMS emissions are calculated using monthly mean seawater concentrations from Kettle and Andreae (2000) and the sea-to-air transfer velocity of Nightingale et al. (2000). Emissions of sea spray (Gong, 2003), primary OC/BC from biofuel and fossil fuel (Bond et al., 2004), and biomass burning OC/BC (Van der Werf et al., 2003) are also included.

2.3 Simulation of mineral dust

The dust model in GLOMAP has not previously been described, so is presented here. The emission flux of dust depends largely on wind speed, vegetation cover and soil characteristics. The sandblasting-saltation scheme of Alfaro and Gomes (2001) is used to parameterize dust emissions in GLOMAP-bin. A horizontal aggregate flux is calculated following White (1979):

$$dF_h(D_p) = (1 - F_{\text{snow}}) \text{PSS} \frac{\rho_p}{g} (u^* - u_t^*(D_p)) (u^* + u_t^*(D_p))^2 dSA_{\text{rel}}(D_p) \quad (1)$$

where F_h is the horizontal aggregate flux ($\text{kg m}^{-1} \text{s}^{-1}$), F_{snow} is the fraction of snow and ice, PSS is the potential source strength, u_t^* is the aggregate threshold friction velocity, u^* is the wind friction velocity calculated at 10 m altitude assuming neutral stability conditions, SA_{rel} is the relative surface area of the saltating aggregate and D_p is the diameter of the soil aggregate. The particle density ρ_p is taken to be 2650 kg m^{-3} and g is the acceleration due to gravity.

Values of F_{snow} are determined from 1998 monthly mean fields provided by ISCCP. PSS is calculated following the method of Lunt and Valdes (2001), and can vary from 0 to 1 depending on the Leaf Area Index (LAI):

Table 1. Soil aggregate size distribution parameters used for each soil texture classification, where n is the fraction of the total aggregate population present in each mode, MMD is the mean aggregate diameter (μm) and σ is a measure of the standard deviation of each mode in the horizontally saltating flux (Zobler, 1986).

Texture	Mode 1			Mode 2			Mode 3		
	n	MMD	σ	n	MMD	σ	n	MMD	σ
Sand	0.9	1000	1.6	0.1	100	1.7	0.1	10.1	1.8
Loamy Sand	0.6	690	1.6	0.3	100	1.7	0.1	10.1	1.8
Sandy Loam	0.6	520	1.6	0.3	100	1.7	0.1	5.1	1.8
Silt Loam	0.5	520	1.6	0.35	100	1.7	0.15	5.1	1.8
Silt	0.45	520	1.6	0.4	75	1.7	0.15	2.5	1.8
Loam	0.35	520	1.6	0.5	75	1.7	0.15	2.5	1.8
Sandy Clay Loam	0.3	210	1.7	0.5	75	1.7	0.2	2.5	1.8
Silty Clay Loam	0.3	210	1.7	0.5	50	1.7	0.2	2.5	1.8
Clay Loam	0.2	125	1.7	0.5	50	1.7	0.3	1.1	1.8
Sandy Clay	0.65	100	1.8	0.1	10	1.8	0.35	1.1	1.8
Silty Clay	0.6	100	1.8	0.1	10	1.8	0.4	0.5	1.8
Clay	0.5	100	1.8	0.1	10	1.8	0.5	0.5	1.8

$$\text{PSS} = \frac{1}{\text{LAI}_{\text{max}}} \cdot (\text{LAI}_{\text{max}} - \text{LAI}) \text{ if } \text{LAI} < \text{LAI}_{\text{max}} \quad (2)$$

else PSS = 0,

where LAI_{max} is equal to 1.2. Monthly mean fields of LAI are taken from International Satellite Land Surface Climatology Project (ISLSCP) data for 1998. ISLSCP generate LAI from observations of the Normalised Difference Vegetation Index measured by the Advanced Very High Resolution Radiometer Instrument.

The ability of the wind to transport soil particles is a function of grain size; large and small particles are poorly mobilized by the wind due to gravitation and cohesive forces, respectively. A soil aggregate undergoes saltation when the surface stress exerted by the wind (wind friction velocity, u^*) exceeds some critical threshold value. The size distribution of the soil aggregates available for saltation is calculated using surface soil texture data from the ISLSCP database. The size distribution of the saltating aggregates assumed when calculating the horizontal aggregate flux is prescribed for each soil texture following Zobler (1986), using the mass median diameter (MMD) and standard deviation (σ) as shown in Table 1 (e.g. Zakey et al., 2006). The aggregate distribution is present in 3 modes, which are implemented across 25 bins in the GLOMAP-bin model. The threshold velocity (u_t^*) required to mobilize each soil aggregate is predicted using the parameterization of Woodward (2001):

$$u_t^* = A \log_{10}(D_p) + B W * C, \quad (3)$$

where $A = -1.2$, $B = 0.5$ and $C = -1.2$, W is the soil moisture contained in the 7 cm deep top soil surface layer (kg m^{-2}). The soil moisture content of the top soil layer is specified from daily ECMWF 40 year re-analysis data for 2001.

Table 2. The geometric mass mean diameter (MMD, μm), geometric standard deviation (σ) and binding energy (e , $\text{kg m}^{-2} \text{s}^{-2}$) of each dust mode used for the vertical sandblasting flux (Clarke et al., 2004).

	Mode 1	Mode 2	Mode 3
MMD	1.06	5.51	14.2
σ	1.46	1.85	1.5
e	3.61×10^{-7}	3.52×10^{-7}	3.46×10^{-7}

It is important to note that the horizontal aggregate flux is not directly injected into the atmosphere as dust. The saltating aggregates inject dust into the atmosphere through the sandblasting process. Fine transportable dust particles are released by surface bombardment from the soil aggregates and/or aggregate breakage. Alfaro et al. (1998) studied dust emissions using wind tunnel experiments with Saharan dust and observed that sandblasting produced 3 dust modes. Alfaro and Gomes (2001) later used a sandblasting model to calculate the kinetic energy of the saltating aggregates in relation to the binding energy of each sandblasted mode. The method of Alfaro and Gomes (2001) is used to parameterize the vertical flux of dust in GLOMAP-bin. Dust is emitted in three lognormal modes which are distributed across the appropriate size bins in the model. To simulate E. Asian dust, we use the lognormal fit parameters recommended by Clarke et al. (2004) as shown in Table 2. Clarke et al. (2004) estimated the geometric mass mean diameter, standard deviation and binding energy of each mode from dust size distributions obtained in the ACE-Asia experiment.

The kinetic energy (e_c , $\text{kg m}^{-2} \text{s}^{-2}$) of each saltating aggregate is calculated following Alfaro and Gomes (2001):

$$e_c = \rho_p \frac{\pi}{12} (D_p)^3 (20 u^*)^2 \quad (4)$$

where ρ_p is the density of dust (2650 kg m^{-3} , assuming composition of CaCO_3). Relative contributions of each mode (P_i) to the vertical dust flux are calculated by comparing the kinetic energy of each saltating aggregate to the binding energy (e_i) of each dust mode (Alfaro and Gomes, 2001). Finally, the vertical number and mass flux are calculated from:

$$dN_i(D_p) = \beta dF_h(D_p) \frac{P_i(D_p)}{e_i} \quad (5)$$

$$dM_i(D_p) = \frac{\pi}{6} \rho_p dN_i(D_p) \bar{d}_i^3 \quad (6)$$

where N_i is the upward vertical number flux of dust in mode i ($\text{m}^{-2} \text{s}^{-1}$), β is a constant (163 m s^{-2}) and M_i is the upward vertical mass flux of dust in mode i ($\text{kg m}^{-2} \text{s}^{-1}$), and \bar{d}_i^3 is the mass mean diameter (Grini et al., 2002).

2.4 Heterogeneous chemistry on dust

Reaction mechanisms and uptake coefficients (γ) for SO_2 differ depending on dust morphology and mineralogy. Knudsen cell experiments measure initial γ (SO_2) ranging from about 10^{-4} (BET surface area) for magnesium and aluminum oxide (Goodman et al., 2001; Usher et al., 2002) to less than 10^{-7} for silica (Usher et al., 2002). Intermediate values have been observed for dust particles from Saharan (10^{-5} – Adams et al., 2005, 10^{-6} – Ullerstam et al., 2003) and Chinese (10^{-5} – Usher et al., 2002) sources, where particles are comprised of many different elements.

Model studies predict that heterogeneous reactions on dust can have a significant impact on the abundance and distribution of SO_2 and sulfate, but the impact is very dependent on the SO_2 uptake coefficient. Bauer and Koch (2005) found that γ (SO_2) $< 10^{-6}$ led to negligible heterogeneous sulfate production on a global scale, while γ (SO_2) = 10^{-3} resulted in the loss of 80% of pure sulfate particles and caused the total global sulfate burden to increase by 15%. A lack of knowledge on the chemical composition of dust derived from different source regions leads to a difference of several orders of magnitude in the uptake coefficient implemented in models. For example, Dentener et al. (1996) and Liao et al. (2004) used γ (SO_2) = 0.1 at $\text{RH} > 50\%$ and a γ (SO_2) = 3×10^{-4} under drier conditions, whilst Bauer and Koch (2005) used γ (SO_2) = 10^{-4} at $\text{RH} > 60\%$ and γ (SO_2) = 10^{-7} at lower humidity.

SO_2 molecules are reversibly adsorbed on the dust surface, but this process is irreversible once the SO_2 is oxidized to form sulfate (Ullerstam et al., 2002; 2003). Goodman et al. (2001) showed that Al_2O_3 and MgO powders became saturated with SO_2 at a surface coverage of 1.5×10^{14} and 4.0×10^{14} molecules cm^{-2} , respectively. There is some evidence that the reactivity of dust can be enhanced under wet

conditions, although this process is poorly understood and will depend on dust mineralogy. Ullerstam et al. (2002) observed a 47% increase in the amount of sulfate formed on dust when samples were exposed to a RH of 80%. Prince et al. (2007) showed that because CaSO_3 undergoes deliquescence and dissolution at a RH of $\sim 90\%$, SO_2 reactions on CaCO_3 are not just limited to the particle surface, but can occur throughout the bulk of the particle, accelerating the production of sulfate. In contrast, Ooki and Uematsu (2005) found that SO_2 reactions on E. Asian dust particles were insensitive to relative humidity over a range of 43–96%.

In our model, SO_2 reacts on the surface of fresh dust (dust in the insoluble distribution) to produce sulfate. Heterogeneous oxidation is limited by the gas phase diffusion rate of SO_2 to the dust surface for the assumed uptake coefficient of SO_2 . Since Asian dust is known to have a strong calcium component (Song and Carmichael, 2001; Song et al., 2003), we use an uptake coefficient $\gamma = 10^{-4}$ based on Knudsen cell experiments with CaCO_3 (Usher et al., 2002). We assume that all SO_2 molecules adsorbed onto dust produce sulfate and that surface saturation occurs once the dust is coated in a mono-molecular sulfate layer. The surface coverage of molecules required to produce a monolayer ($1.6 \times 10^{14} \text{ cm}^{-2}$) lies in the range of measurements of the number of molecules required to completely exhaust active sites on the dust surface (Goodman et al., 2001). We do not consider reactivation of saturated dust surfaces at high humidity.

2.5 Model setup

The model was spun up over a 7 week period prior to 6 April 2001 and then run for a further 10 days (6–15 April) to simulate the largest dust storms observed in the ACE-Asia experiment. Simulations were performed with and without dust and are referred to as the DUST and NODUST experiments.

3 Observations and analysis statistics

We evaluate modeled aerosol concentrations against observations from the Aerosol Characterization Experiment-Asia (ACE-Asia) field campaign (Huebert et al., 2003; Seinfeld et al., 2003). The experiment was conducted in E. Asia from late March to early May 2001 to coincide with the Asian dust storm season. Detailed observations of aerosols and trace gases were made by 3 aircraft, 2 ships and at a number of ground sites. In this study we focus on the largest dust storms that occurred from 6–15 April. These dust storms were intercepted by the NCAR C-130 aircraft after the dust had mixed with pollution from three of the largest cities in E. Asia (Beijing, Tianjin and Seoul). Here, we compare modeled DUST and NODUST aerosol concentrations and size distributions with data from 3 flights over the Yellow

Sea: RF06 (11 April), RF07 (12 April) and RF08 (13 April). GLOMAP model output was interpolated along the trajectory of each flight at 1 minute intervals. Observed and modeled results are at standard temperature and pressure (STP, 298 K and 1013 hPa). The approximate location of the analyzed flights is shown by a white box in Fig. 4a.

Dust mass concentrations were not directly measured in the ACE-Asia experiment. We estimate the mass concentration of dust sampled in each C-130 flight from size-resolved measurements of particle number concentration obtained by the Thermo-Optic Aerosol Discriminator (TOAD), which operated over a particle size range of 120 nm to 12 μm diameter. Aerosol samples were averaged over 30 s periods and intermittently heated to temperatures in excess of 300 °C to evaporate volatile aerosol, leaving refractory components (Clarke et al., 2004). Because refractory aerosol concentrations were dominated by dust during the dust storm, we have converted the refractory aerosol size distribution into a total mass concentration assuming a dust particle density of 2650 kg m⁻³ (representing CaCO₃). It should be noted that the estimated dust concentrations are uncertain within at least a factor of 2 due to problems with sizing dust particles using optical methods (Clarke et al., 2004; Tang et al., 2004a). The resulting mass concentrations have been reduced by a factor of 1.7 to account for the fact that dust particles are over-sized by the TOAD instrument (Clarke et al., 2004).

Fine sulfate mass concentrations ($D_p < 1.3 \mu\text{m}$) were sampled on the C-130 aircraft as sulfate ions by a Particle In Liquid Sampler (PILS) at 3 min intervals. Coarse ($D_p > 1.0 \mu\text{m}$) sulfate concentrations were measured on the C-130 aircraft by a micro-orifice impactor (MOI) over 20 to 70 min periods (Huebert et al., 2003). The MOI sampled ions across 5 stages with 50% upper cutoff diameters of 5.0, 1.4, 0.77, 0.44 and 0.25 μm .

SO₂ concentration measurements were made on the C-130 aircraft by an Atmospheric Pressure Ionisation Mass Spectrometer (APIMS) with a time resolution of 1 s.

Total particle number concentrations (>3 nm diameter) were sampled on the C-130 aircraft by a CN counter with a time resolution of 1 s.

Particle size distributions were obtained on the C-130 aircraft by a differential mobility analyzer (DMA) as well as the TOAD instrument. The DMA measured the aerosol size distribution across an approximate size range of 8–120 nm diameter over 1 min intervals. TOAD operated over a 30 s sampling period, and provided additional size information between 120 nm and 12 μm diameter (Clarke et al., 2004).

Model performance against the observations was assessed in terms of the Taylor skill score (S), model bias (B), and proportion of model values within a factor of 2 (P_2) and 10 (P_{10}) of the measured concentrations. Modeled aerosol concentrations are averaged over the same sampling (averaging) period of each individual observation to calculate S , P_2 and P_{10} . The number of data points used to produce the statistical data (N) is given for each flight. The model bias (B)

is the ratio of the mean modeled concentration to the mean observed concentration. The Taylor skill score (S) gives the correlation between the structure and magnitude of variability modeled and observed (Taylor et al., 2001):

$$S = \frac{4(1+R)}{\left(\sigma_f + \frac{1}{\sigma_f}\right)^2 (1+R_0)}, \quad (7)$$

where R is the correlation coefficient, R_0 is the maximum attainable correlation coefficient, and σ_f is the ratio of model standard deviation to that of the observation. R_0 is assumed to be 1, although in reality uncertainties in measurements and the coarse resolution of the model would result in an R_0 value less than 1. S approaches 1 as R increases to R_0 and as the model variance approaches the variance observed.

4 Analysis of aerosol and precursor gas masses

4.1 Dust

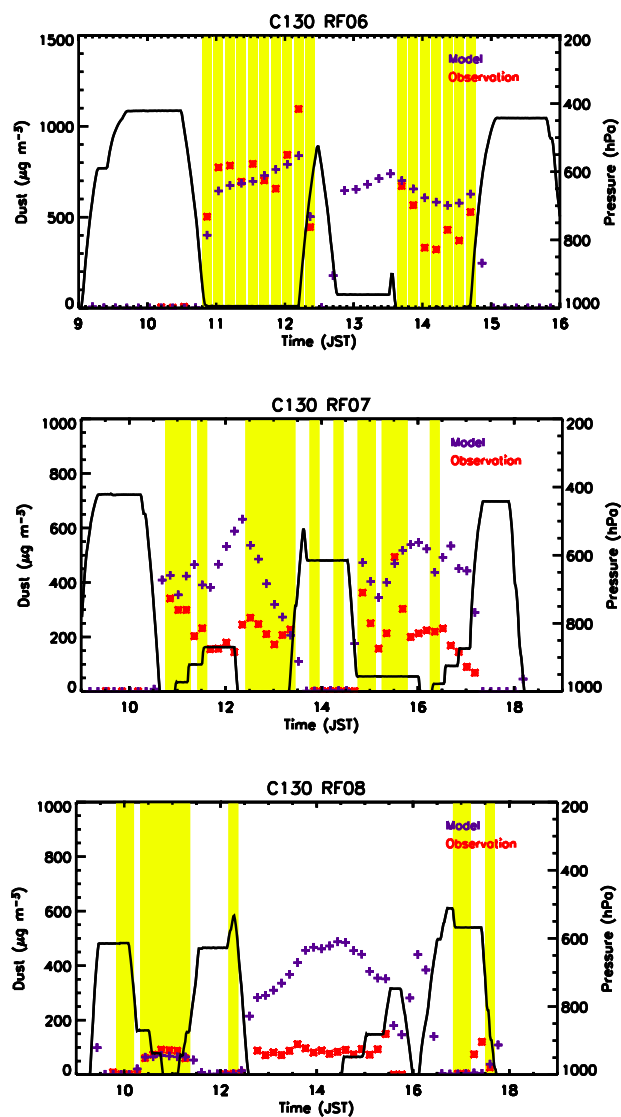
4.1.1 Dust during observation periods

The dust-storm simulated in this study occurred as two separate events. The first was generated on 6 April when a cold front passed across Inner Mongolia and the Gobi and Taklimakan deserts. The dust cloud was transported towards northeast China, reaching Japan on 8 April. The second dust episode was initialized over Mongolia on 8/9 April and was dispersed towards the east, arriving at the Sea of Japan and Yellow Sea on 10 April. The dust loading and size distribution produced during these events will control the total surface area available for reactions with sulfur species. Before we use GLOMAP-bin to perform a detailed analysis of dust-sulfate interactions, it is important to adequately simulate the dust concentrations observed over this period.

We find that the original dust-parameterization underestimates dust concentrations by up to an order of magnitude during each flight (not shown). The disagreement may be related to the dust parameterization used, an underprediction of the wind strength across the Gobi and Taklimakan deserts (Tegen et al., 2002), underprediction of peak wind speeds in ECMWF (Middleton, 1986) or unresolved sub-grid variability in the wind speed. modeled dust emissions were therefore adjusted across grid boxes corresponding with the E. Asian dust source (30–60° N and 75–140° E) to best reproduce the dust concentrations observed by the TOAD instrument. The vertical number flux of dust ($dN_i(D_p)$), Eq. (5) was increased on specific days by the factors shown in Table 3. The dust adjustment factors selected were chosen from a sensitivity study in which the dust flux was adjusted and compared against TOAD observations. The tuning of dust emissions is justifiable in this study since the dust storm has been simulated only for the purpose of examining the impact of dust on tropospheric sulfur species.

Table 3. The daily factor of increase applied to the vertical number flux of dust relative to an initial baseline simulation.

Date	Factor of increase	Date	Factor of increase
1–31 March	7.0	1–7 April	9.0
8 April	14.0	9 April	10.0
10–15 April	6.0		

**Fig. 1.** Dust mass concentrations derived from OPC-TOAD 300C size distribution (red) and modeled (purple) for C-130 flights 6, 7 and 8. The yellow shading covers time periods where dust is simulated within a factor of 2 of the concentrations observed. The altitude (pressure; hPa) of the aircraft is denoted by the black line. Results are at STP. JST is Japan Standard Time (GMT+9 h).**Table 4.** Model analysis of observed dust mass concentrations. The number of model-observation points (N), model bias (B), Taylor skill score (S) and fraction of dust concentrations simulated within a factor of 2 (P_2) and 10 (P_{10}) of observations from the C130 aircraft. N , B , S , P_2 and P_{10} are defined in Sect. 2.

Flight #	N	B	S	P_2	P_{10}
C-130 flight 6	20	1.0	0.93	85	85
C-130 flight 7	40	2.0	0.68	45	90
C-130 flight 8	37	3.4	0.14	32	89

The dust mass concentrations simulated and observed on C-130 flights 6, 7 and 8 are presented in Fig. 1 averaged over 10 min periods. The model-observation agreement is shown in Table 4. Flight 6 occurred over the Yellow Sea on 11 April, intercepting a dust-laden air mass that had traveled at low altitudes (<500 m) from the Gobi desert through Beijing as well as other urban centers in China (Song et al., 2007). The dust mass sampled in this flight peaked at concentrations >1000 $\mu\text{g m}^{-3}$. GLOMAP-bin simulates 85% of the dust concentrations observed in flight 6 within a factor of 2 of measurements from the TOAD instrument and captures the variability in dust with a skill score of 0.93. Measured dust concentrations decreased to less than 600 and 300 $\mu\text{g m}^{-3}$ in flights 7 (12 April) and 8 (13 April) respectively, as the second dust storm began to disperse and move beyond the Yellow Sea. The model captures the variability in the concentrations measured in flight 7 ($S=0.68$) but over-predicts the average dust loading by a factor of 2. Similarly, concentrations are overestimated by approximately a factor of 3–5 for a substantial portion of flight 8.

In order to reliably represent the total dust surface available for reactions with sulfur species, we have restricted our analysis to flight periods when dust concentrations are modeled within a factor of 2 of observations (shown in yellow in Fig. 1). These periods are: 1045–1230 and 1330–1445 JST in flight 6, 1045–1145, 1230–1330 and 1445–1545 JST in flight 7 and 0945–1130 JST in flight 8. Although modeled dust mass concentrations are within factor of 2 of the observations during these periods, it is important to note that total surface area of dust will also be governed by how this mass is distributed across the particle size distribution. More than 98% of modeled dust existed at particles sizes greater than 400 nm diameter during all three flights. Figure 9 shows that the number size distribution of particles modeled from 0.4–10 μm is in reasonable agreement with observations from the TOAD instrument in flights 7 and 8. The number of dust particles modeled at sizes between 0.7–5 μm is overestimated by up to a factor of 3 in flight 6, but is under-predicted at larger sizes. A further uncertainty that we do not attempt to evaluate here is the effect of errors in the deposition rate between dust emission and interception. If modeled dust deposition rates were in error then the dust could have a larger or smaller impact on sulfate than we estimate here.

Table 5. Model analysis of observed fine sulfate mass concentrations. The number of model-observation points (N), model bias (B), Taylor skill score (S) and fraction of fine sulfate concentrations simulated within a factor of 2 (P_2) and 10 (P_{10}) of observations from the C130 aircraft in the DUST experiment. Results for the NODUST simulation are shown in parentheses.

Flight #	N	B	S	P_2	P_{10}
C-130 flight 6	44	0.79 (0.91)	0.86 (0.85)	91 (91)	98 (100)
C-130 flight 7	45	0.65 (0.7)	0.73 (0.76)	80 (87)	100 (100)
C-130 flight 8	27	0.96 (0.98)	0.97 (0.97)	63 (63)	100 (100)

4.2 Sulfate

4.2.1 Fine sulfate during observation periods

The presence of dust would be expected to reduce fine sulfate by coagulation scavenging of sulfate particles, suppression of new particle formation and by acting as a sink for H_2SO_4 vapor that would otherwise condense on the smaller particles. ACE-Asia observations from the C-130 aircraft suggested that this effect may have occurred during the Asian dust storm. Clarke et al. (2004) demonstrated that the combined mass of fine sulfate, nitrate and ammonium was at its highest when the coarse mode ($D_p > 1 \mu\text{m}$) concentration was about $80 \mu\text{m}^3 \text{cm}^{-3}$, but was about 50% lower when the coarse mode concentration exceeded $500 \mu\text{m}^3 \text{cm}^{-3}$. The DUST and NODUST simulations performed here allow us to estimate how dust modified the concentration of fine sulfate sampled during the dust storm.

Fine sulfate mass concentrations measured and modeled in the DUST and NODUST simulation are shown in Fig. 2. Note that in the DUST simulation, fine sulfate includes pure sulfate particles as well as sulfate present on fine dust. Table 5 shows that for flights 6, 7 and 8 respectively, 91%, 80% and 63% of the fine sulfate concentrations simulated in the DUST experiment are predicted within a factor of 2 of measurements from the PILS instrument. The model also achieves high (>0.7) skill scores for each C-130 flight, which suggests that the variability in concentrations is captured well by the model.

When we compare results from the DUST and NODUST experiments, we find that the presence of dust reduces modeled fine sulfate concentrations by 9%, 4% and 1% in flights 6, 7 and 8, respectively. These changes reflect the net effect of increases in fine sulfate associated with fine dust particles and possible decreases in pure sulfate particle mass. Fine sulfate is under-estimated in the DUST experiment, hence the neglect of dust leads to an improvement in model bias for each flight, although the model bias remains less than 1. Our results can be compared with those of Tang et al. (2004b) who used the STEM-2K3 regional model to examine how dust modified fine sulfate in the same flights

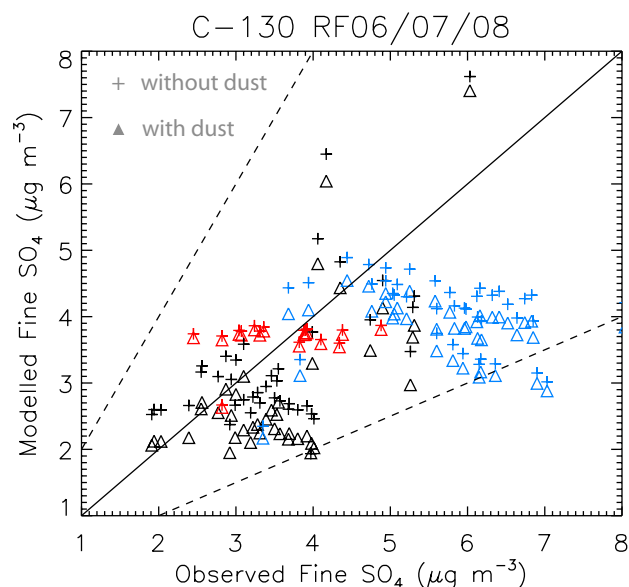


Fig. 2. Fine sulfate ($D_p < 1.3 \mu\text{m}$) mass concentrations modeled and observed by the PILS instrument for C-130 flights 6 (black), 7 (blue) and 8 (red). Modeled concentrations are shown for the DUST (triangle) and NODUST (cross) simulations. Results are at STP.

as studied here. They predicted that dust had little influence on fine sulfate throughout flights 7 and 8, but led to a 30% increase in fine sulfate throughout periods of flight 6 following sulfate production on fine dust particles. The disagreement between studies probably reflects differences in the competing effects modeled between sulfate production on sub-micron dust and loss of pure fine sulfate particles to super-micron dust.

We can estimate the amount of sulfate produced on fine dust from the change in sulfate modeled at particle sizes where dust is present. Less than 2% of the mass of dust modeled and sampled by the TOAD instrument existed at sizes $<400 \text{ nm}$ diameter. Model sulfate concentrations at sizes $<400 \text{ nm}$ decrease by approximately $1.3 \mu\text{g m}^{-3}$ (45%), $0.6 \mu\text{g m}^{-3}$ (16%) and $0.08 \mu\text{g m}^{-3}$ (4%) in flights 6, 7 and 8 respectively, following scavenging of sulfur onto sub and super-micron dust. But there is an increase of $0.92 \mu\text{g m}^{-3}$ (985%), $0.3 \mu\text{g m}^{-3}$ (284%) and $0.04 \mu\text{g m}^{-3}$ (72%) in modeled sulfate from $0.4\text{--}1.3 \mu\text{m}$ in each of the same flights, due to SO_4 production on fine dust particles. We calculate that approximately 33%, 9% and 2% of simulated fine sulfate is associated with dust in flights 6, 7 and 8, respectively. These figures are consistent with the work of Maxwell-Meier (2004), who estimated from PILS data that approximately 20% of fine sulfate was associated with calcium (dominant cation component in Asian dust) in C-130 flight 6, and that an even smaller fraction was associated with calcium in flight 7. So we conclude that although up to 30% of modeled fine sulfate was produced on dust particles during

Table 6. Model analysis of observed coarse sulfate mass concentrations. The number of model-observation points (N), model bias (B), Taylor skill score (S) and fraction of coarse sulfate concentrations simulated within a factor of 2 (P_2) and 10 (P_{10}) of observations from the C-130 aircraft in the DUST experiment. Results for the NODUST simulation are shown in parentheses.

Flight #	N	B	S	P_2	P_{10}
C-130 flights	20	0.6 (0.05)	0.15 (0.001)	75 (0)	95 (40)

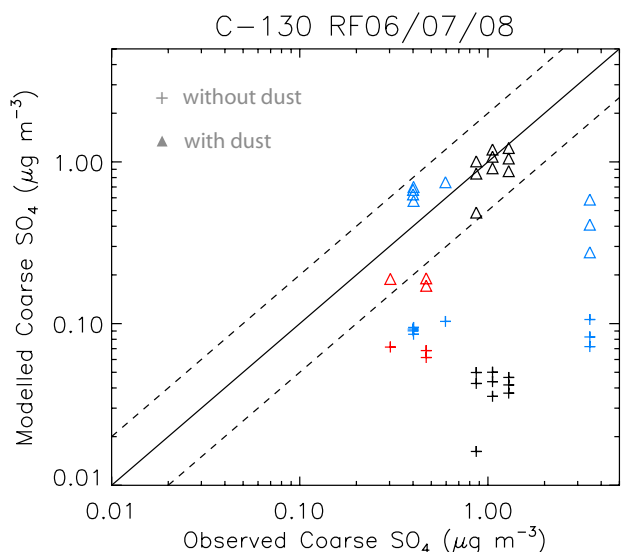


Fig. 3. Coarse sulfate ($D_p > 1 \mu\text{m}$) mass concentrations modeled and observed by the MOI instrument for C-130 flights 6 (black), 7 (blue) and 8 (red). Modeled concentrations are shown for the DUST (triangle) and NODUST (cross) simulations. Results are at STP.

each C-130 flight, the presence of dust acted to redistribute the sulfate from smaller to larger particles, with the net effect of reducing fine sulfate concentrations by up to 10%.

4.2.2 Coarse sulfate during observation periods

Observed and modeled coarse sulfate mass concentrations from flights 6, 7 and 8 are shown in Fig. 3 for the DUST and NODUST simulation. Table 6 shows that in the DUST experiment 75% of modeled coarse sulfate concentrations are within a factor of 2 of the observations. However, the maximum observed coarse sulfate concentration of $3.5 \mu\text{g m}^{-3}$ during flight 7 is under-predicted by up to an order of magnitude so the overall model bias is 0.6 and the skill score is only 0.15. Figure 3 and Table 6 show that the agreement between modeled and observed coarse sulfate concentrations decreases markedly when dust is removed from the model. In the NODUST experiment, the model bias and skill score decrease to 0.05 and 0.001, respectively, and none of the

modeled concentrations are predicted within a factor of 2 of the observations. These results indicate that dust was important for controlling the concentration of coarse sulfate during the dust event, and suggest that GLOMAP-bin provides a reasonable prediction of the rate of sulfate formation on coarse dust particles.

4.2.3 Regional impacts of dust on total sulfate

The presence of dust reduces the average sulfate mass concentration modeled in flights 6, 7, and 8 by up to 10% ($0.42 \mu\text{g m}^{-3}$) at sizes below $1.3 \mu\text{m}$ diameter, but leads to a relative increase in sulfate of up to an order of magnitude ($0.47 \mu\text{g m}^{-3}$) at larger sizes. These two effects compensate, leading to the small overall increase in total sulfate of less than 2% in each C-130 flight.

Aircraft observations were confined to the Yellow Sea and Sea of Japan, downwind from regions where dust-sulfate interactions may be much larger than the regional average. The average boundary layer ($< 1 \text{ km}$) concentration of total sulfate modeled across E. Asia in the dust storm period (6–14 April) is shown for the NODUST simulation in Fig. 4a. Total sulfate mass concentrations peak at approximately $6\text{--}20 \mu\text{g m}^{-3}$ across E. China, Korea and Japan. Figure 4b shows that total sulfate concentrations increase by less than 4% across these regions following interactions with dust. The largest relative increase in sulfate is simulated over desert source regions. Sulfate mass concentrations rise by over 40% across the Gobi desert, although this corresponds with an absolute increase of less than $0.2 \mu\text{g m}^{-3}$.

4.3 Gas phase sulfur species

4.3.1 SO_2 during observation periods

Measured SO_2 concentrations have been averaged over 1 min intervals and are shown together with modeled SO_2 from the DUST and NODUST experiments in Fig. 5. Modeled SO_2 concentrations are typically under-predicted by 30–55% (Table 7). SO_2 was extremely variable in each flight, and GLOMAP is unable to capture the variability in the concentrations observed ($S=0.19\text{--}0.5$), probably due the coarse resolution of the model.

The direct uptake of SO_2 onto mineral dust particles will deplete SO_2 concentrations. However, comparison of the DUST and NODUST experiments (Fig. 5 and Table 7) shows that the dust has negligible influence on SO_2 . In our model, heterogeneous oxidation of SO_2 is limited because of surface saturation effects once the dust becomes coated. When the dust plume reaches the Yellow Sea, nearly all dust particles are coated in a monolayer of sulfate since they have passed over E. Asian megacities and so are unreactive with SO_2 by that time. In Sect. 4.3.2 we show that the observed abundance of sulfate on coarse dust can be explained instead by condensation of H_2SO_4 vapor.

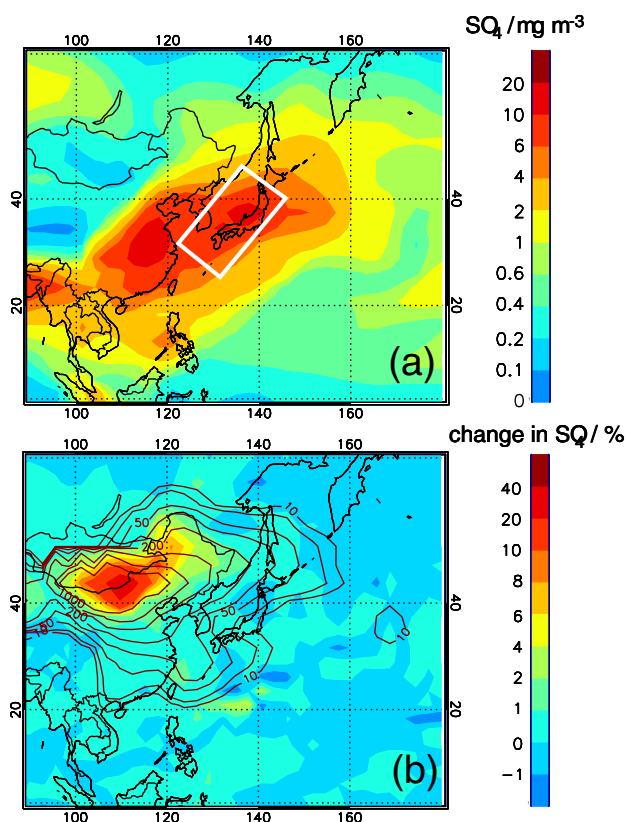


Fig. 4. (a) Mean model total mass concentration of particulate sulfate below 1 km altitude during the dust storm (6–14 April) for the NODUST simulation, (b) percentage change in sulfate following the inclusion of dust. Brown isopleths show the mean boundary layer concentration of dust ($\mu\text{g m}^{-3}$) simulated over the PDS period. The white box in (a) shows the approximate location of the C-130 flights (Huebert et al., 2003)

4.3.2 Regional impacts of dust on SO_2 and H_2SO_4

The average boundary layer (<1 km) concentration of SO_2 and $\text{H}_2\text{SO}_4(\text{g})$ modeled over E. Asia in the dust storm period (6–15 April) is shown for the NODUST simulation in Fig. 6. The relative change in SO_2 and H_2SO_4 is also shown when dust is included.

Maximum simulated SO_2 concentrations (2000–10 000 pptv) occur over Korea, Japan and eastern China. The Yellow Sea and Sea of Japan are also heavily influenced by SO_2 from these regions. The presence of dust reduces boundary layer SO_2 by less than 0.2% over the Yellow Sea and Sea of Japan, as seen in the interpolations for the C-130 aircraft. The largest relative change in SO_2 occurs across the Gobi desert, although the reduction is typically <10%.

Gas phase H_2SO_4 is produced from the oxidation of SO_2 by OH, and H_2SO_4 concentrations have a similar spatial distribution to SO_2 (Fig. 6). But dust has a larger impact on modeled gas phase H_2SO_4 than predicted for SO_2 . Boundary layer concentrations are reduced by up to 80% across

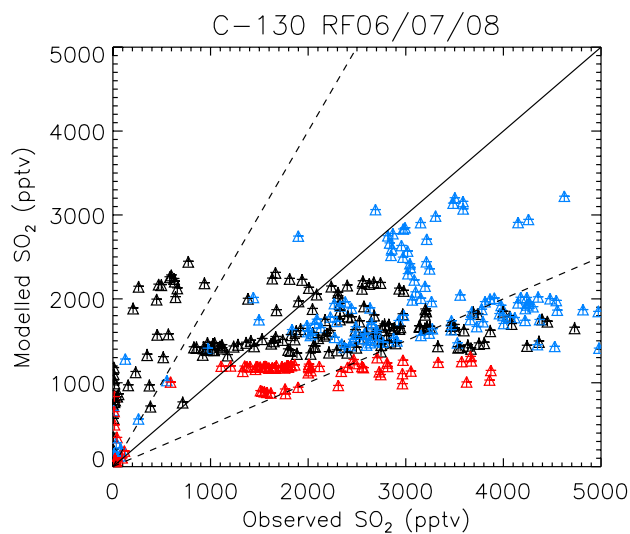


Fig. 5. SO_2 mixing ratios modeled and observed for C-130 flights 6 (black), 7 (blue) and 8 (red). Modeled concentrations are shown for the DUST (triangle) and NODUST (cross) simulations.

Table 7. Model analysis of observed SO_2 concentrations. The number of model-observation points (N), model bias (B), Taylor skill score (S) and fraction of SO_2 concentrations simulated within a factor of 2 (P_2) and 10 (P_{10}) of observations from the C-130 aircraft in the DUST experiment. Results for the NODUST simulation are shown in parentheses.

Flight #	N	B	S	P_2	P_{10}
C-130 flight 6	178	0.71 (0.71)	0.19 (0.19)	59 (60)	90 (90)
C-130 flight 7	164	0.45 (0.45)	0.11 (0.11)	52 (52)	96 (96)
C-130 flight 8	107	0.58 (0.58)	0.50 (0.50)	39 (39)	97 (97)

S. Mongolia and N. China, and by 10–20% across the Yellow Sea. Lee et al. (2009) used the GISS-TOMAS model to also demonstrate that dust severely depletes gas phase H_2SO_4 concentrations in dusty regions. They simulated much lower dust concentrations over E. Asia (<100 $\mu\text{g m}^{-3}$) than observed and simulated here, but predicted that dust depleted H_2SO_4 by up to 30% across China.

Condensation of H_2SO_4 on dust is not affected by the amount of sulfate present on the dust surface. This allows both fresh and chemically aged dust to remove gaseous H_2SO_4 and produce sulfate. Analysis of the modeled sulfur budget for atmospheric columns where the dust concentration exceeded 200 mg m^{-2} (over the dust storm period) shows that heterogeneous oxidation of SO_2 produced 0.06 $\text{mg m}^{-2} \text{d}^{-1}$ of SO_4 compared to 1.83 $\text{mg m}^{-2} \text{d}^{-1}$ for condensation of H_2SO_4 . We therefore find that the sulfate associated with dust during the dust storm originated largely from the uptake of H_2SO_4 , and is sufficient to explain the observed coarse sulfate.

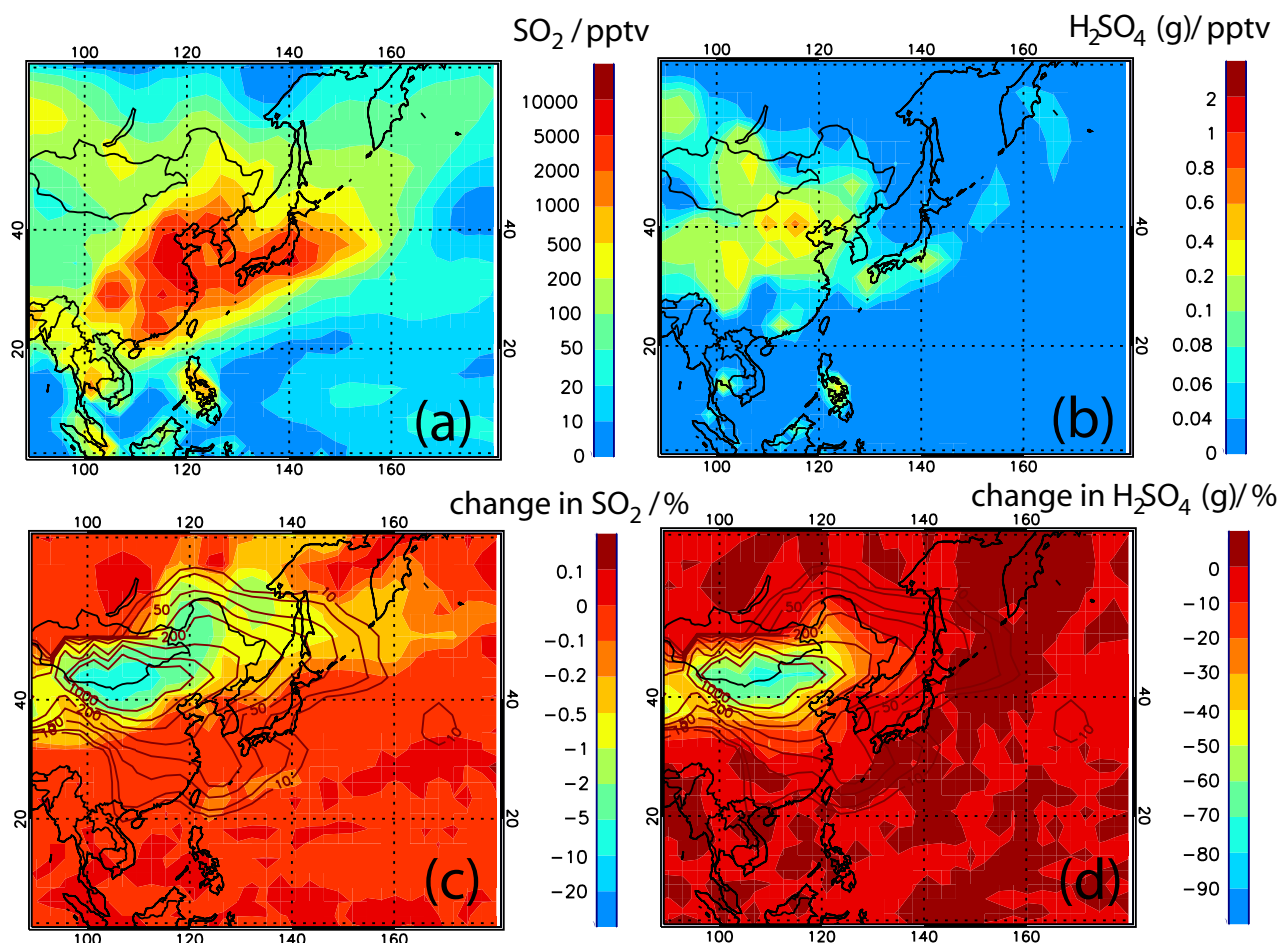


Fig. 6. Mean gas phase SO_2 and H_2SO_4 mixing ratios modeled in the boundary layer (<math><1\text{ km}</math>) over the dust storm period (6–15 April). (a) SO_2 in the NODUST simulation, (b) H_2SO_4 in the NODUST simulation, (c) percentage change in SO_2 following inclusion of dust, (d) percentage change in H_2SO_4 following inclusion of dust. Brown isopleths show the mean boundary layer concentration of dust ($\mu\text{g m}^{-3}$) over the same period.

4.4 Comparison with previous studies

The amount of sulfate produced on dust depends on dust surface area and chemistry, the concentration of sulfur species, as well as the environmental conditions. SO_2 uptake coefficients differ by many orders of magnitude between studies, and there are differing assumptions about the reactivity of dust particles (Sect. 2.4). Dentener et al. (1996) estimated that the presence of dust increased sulfate mass concentrations by 10–20% across the Yellow Sea and Sea of Japan. Xiao et al. (1997) predicted that dust caused an increase in the sulfate mass concentration of over 40% in the PEM West B campaign, leading to a coarse sulfate fraction of 70% across the east coast of China. Song and Carmichael (2001) performed a similar study to Xiao et al. (1997) and simulated a 40% increase in sulfate, and a coarse sulfate fraction of 30–60% in a dust plume over the Yellow Sea. Approximately 10–30% of the sulfate

mass was observed at super-micron sizes in flights 6, 7 and 8 of the ACE-Asia experiment. Most of the ACE-Asia observations were made at dust concentrations of 100–1000 $\mu\text{g m}^{-3}$, which are a factor 10–100 greater than simulated by Dentener et al. (1996), Xiao et al. (1997) and Song and Carmichael (2001). These studies did not consider surface saturation effects when modeling heterogeneous reactions between SO_2 and dust, which allowed SO_2 to be continually oxidized to sulfate on the dust surface. If these studies had simulated the uptake of sulfur species onto the large dust surface observed during ACE-Asia then they would probably have greatly overestimated the coarse sulfate fraction observed in the ACE-Asia campaign.

The depletion of SO_2 calculated by Tang et al. (2004a) also seems to be inconsistent with our model and the observations. They used the STEM-2K1 regional model to examine heterogeneous reactions between SO_2 and dust over the ACE-Asia campaign. They did not consider surface

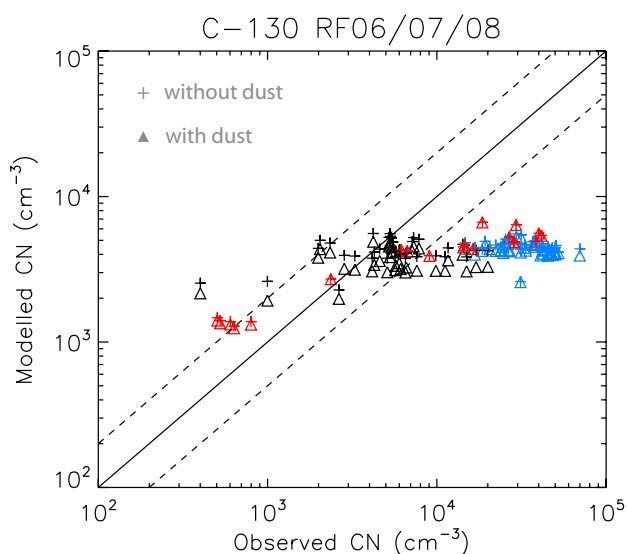


Fig. 7. CN concentrations modeled and observed by the CN counter for C-130 flights 6 (black), 7 (blue) and 8 (red). Modeled concentrations are shown for the DUST (triangle) and NODUST (cross) simulations. Results are at STP.

saturation effects and estimated that SO_2 concentrations were reduced by 1–15% across the Yellow Sea when averaged over the dust storm period, and by as much as 1000 pptv throughout C-130 flight 6. 1000 pptv SO_2 is equivalent to $4.1 \mu\text{g m}^{-3}$ of sulfate at STP. Approximately 90% of the dust surface existed at super-micron sizes during this flight so depletion of 1000 pptv SO_2 would equate to $\sim 3.7 \mu\text{g m}^{-3}$ coarse particle sulfate. The equivalent depletion of SO_2 in GLOMAP-bin would worsen the model bias for SO_2 from 0.71 to 0.25 and would cause a factor of 3–4 overprediction of the coarse sulfate concentration (compared with the 40% bias between modeled and observed coarse SO_4 with limited oxidation of SO_2 on dust, Table 6).

We find that the sulfate associated with dust during the ACE-Asia campaign most likely originated from the condensation of H_2SO_4 , which, unlike SO_2 , is not influenced by the mixing state of dust (Sect. 4.3). Our uptake of SO_2 is limited to a monolayer on the dust surface, which greatly reduces the amount of sulfate produced via heterogeneous oxidation. If the total oxidation of SO_2 on dust were as large as in previous studies we would significantly underestimate SO_2 and overestimate the amount of sulfate associated with dust. Our results indicate that the amounts of SO_2 oxidized on dust have been overestimated in previous studies. This conclusion is consistent with a study by Song et al. (2007), who demonstrated that large amounts of CO_3^{2-} were present in fine dust particles transported in E. Asian outflow. Carbonate is displaced by acidic species such as sulfate and nitrate, so can provide information on the chemical age of dust. Song et al. (2007) estimated that respectively, 87%, 68% and 39% of CO_3^{2-} remained in the fine dust particles sampled by

Table 8. Model analysis of observed CN concentrations. The number of model-observation points (N), model bias (B), Taylor skill score (S) and fraction of CN concentrations simulated within a factor of 2 (P_2) and 10 (P_{10}) of observations from the C-130 aircraft in the DUST experiment. Results for the NODUST simulation are shown in parentheses.

Flight #	N	B	S	P_2	P_{10}
C-130 flight 6	36	0.54 (0.65)	0.06 (0.06)	67 (67)	100 (100)
C-130 flight 7	36	0.12 (0.13)	0.002 (0.002)	0 (0)	67 (75)
C-130 flight 8	20	0.24 (0.24)	0.05 (0.05)	25 (20)	100 (100)

C-130 flights 6, 7 and 8 in the ACE-Asia experiment. They used a Lagrangian photochemical box model to show that such a large CO_3^{2-} fraction in dust could only be reproduced if the rate of SO_2 oxidation on dust was significantly slower than estimated in previous models.

5 Analysis of particle number concentrations

The reduction in the mass concentration of fine sulfate simulated in the presence of dust (Sect. 4.2.1) suggests that dust influences the existing aerosol. The influence can occur through coagulation scavenging of small particles or removal of H_2SO_4 vapor leading to reduced condensation on existing aerosol and a reduction in new particle formation. Lee et al. (2009) used the GISS-TOMAS global aerosol microphysical model to demonstrate that dust can either enhance or deplete total CCN concentrations depending on the size distribution of dust emissions. As discussed in Sect. 4.1.1, the mass concentration and size distribution of dust modeled here are in reasonable agreement with observations from the TOAD instrument and should therefore provide a reasonable representation of the impact of dust on the aerosol size distribution. Dust impacts on the total particle concentration (CN) and concentration of particles at CCN sizes observed in the ACE-Asia campaign have not been examined in previous studies. In this section we evaluate CN and CCN number concentrations against observations from the C-130 aircraft following the simulation and elimination of dust.

5.1 Total particle number concentrations

5.1.1 CN during observation periods

Measured CN concentrations have been averaged over 5 min intervals here. Observed and modeled CN concentrations from flights 6, 7 and 8 are presented in Fig. 7 for the DUST and NODUST simulation.

Table 8 shows that in the DUST experiment, the model is within 50% of the observations in flight 6 but underpredicts CN concentrations by about 90% throughout flight 7, and 80% throughout flight 8. Observations revealed that these

particles may have been produced through ternary nucleation of NH_3 , H_2SO_4 and H_2O (McNaughton et al., 2004). Only binary H_2SO_4 - H_2O nucleation has been considered in this simulation. Furthermore, nucleation rates are strong nonlinear functions of temperature and precursor gas vapor pressures. Sub-grid scale variations in humidity, temperature or H_2SO_4 concentration could lead to higher nucleation rates than predicted using large scale average grid values.

We find that the presence of dust leads to a reduction in mean modeled particle concentration of 827 cm^{-3} (20%), 375 cm^{-3} (8%) and 34 cm^{-3} (1%) at sizes below 400 nm in flights 6, 7 and 8, respectively, which is only partially compensated for by the presence of dust at larger sizes. CN concentrations decrease by 729 cm^{-3} (17%), 282 cm^{-3} (6%) and 32 cm^{-3} (1%) in flights 6, 7 and 8, respectively. The dust storm therefore resulted in the net loss of CN, despite being a source of primary particles. These reductions in CN might have been larger for flights 7 and 8 if our model simulated the much higher concentrations of smaller particles that were observed, because of scavenging of small nuclei by the dust.

5.1.2 Regional impacts of dust on CN

Average boundary layer (<1 km) CN concentrations modeled in the dust storm period are presented in Fig. 8a. The model predicts CN concentrations $>6000 \text{ cm}^{-3}$ across E. China, Korea and Japan. Throughout the Yellow Sea and Sea of Japan, simulated CN concentrations are typically $>2000 \text{ cm}^{-3}$. Figure 8b shows that dust reduces modeled boundary layer CN concentrations by less than 5% across E. China, Korea and Japan. Observations of particle concentrations from Seoul, Korea (Chun et al., 2001) and Toyama, Japan (Watanabe et al., 2006) have also shown that total CN are barely depleted during heavy dust storm events. The largest relative change in modeled CN occurs across N. China and Mongolia, i.e. source regions of dust. CN are reduced by up to 20% across these regions, although CN concentrations are substantially smaller here (1000 – 4000 cm^{-3}) than across E. China (6000 – $20\,000 \text{ cm}^{-3}$).

5.2 Cloud condensation nuclei

5.2.1 CCN during observation periods

At low to moderate cloud supersaturations of 0.3%, particles as small as 50 nm dry diameter can act as CCN. Here we investigate dust impacts on CCN-sized particles by evaluating the change in the aerosol size distribution between the NODUST and DUST simulation.

The average particle size distribution modeled and observed during each flight is shown in Fig. 9. In the DUST simulation, the observed size distribution is reproduced extremely well at super-micron sizes in flights 7 and 8. Aerosol in this size range is predominantly dust, suggesting that the

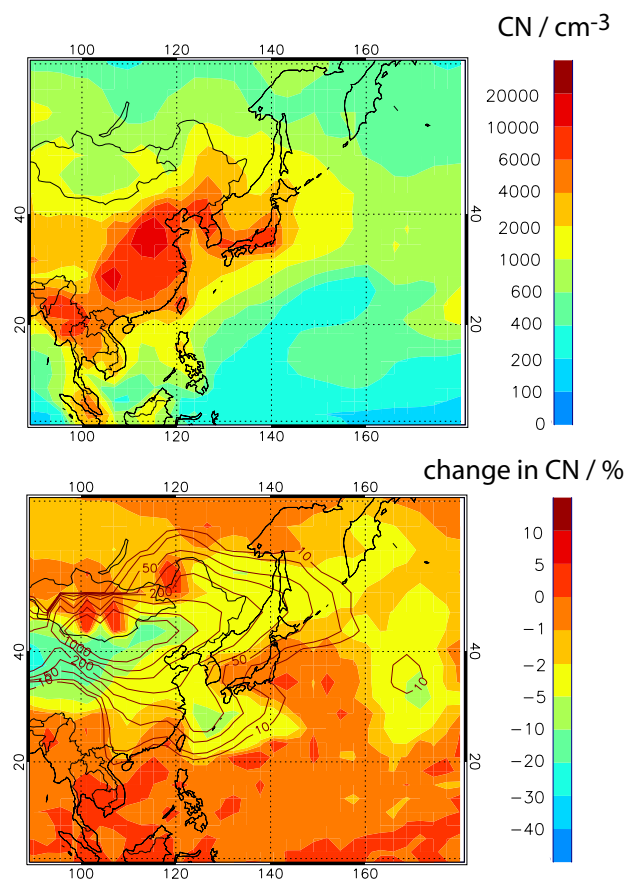


Fig. 8. (a) Mean boundary layer CN concentrations modeled for 6–14 April in the NODUST simulation. (b) The percentage change in simulated CN following the inclusion of dust. Brown isopleths show the average boundary layer dust loading ($\mu\text{g m}^{-3}$) simulated over the dust storm period.

model provides a good representation of the dust surface available for interactions with sulfur species. Aerosol below 400 nm diameter is comprised largely of sulfate, sea-salt, BC and OC. The model reliably predicts the particle size distribution from 20–400 nm in flights 6 and 8, but underpredicts particle concentrations by up to a factor of 5 at 20–90 nm in flight 7. Particle concentrations below 20 nm are underestimated in all 3 flights, which is consistent with an underprediction of the CN concentration (Fig. 7) following a particle formation event.

In order to examine the influence of dust on CCN-sized particles, we quantify changes in the concentration of particles >50 nm dry diameter between both model experiments. Soluble particles in this size range would activate at low to moderate cloud supersaturations of 0.3%. Table 9 shows the change in CCN in two size categories: N_{50-400} and $N_{>50}$. Since less than 2% of the mass of dust is emitted below 400 nm diameter in the model, N_{50-400} is dominated by non-dust particles while $N_{>50}$ includes dust. As an upper limit

Table 9. Absolute and percentage changes (parentheses) in particle concentration modeled between the NODUST and DUST simulation at sizes from 50 to 400 nm (N_{50-400}) and above 50 nm ($N_{>50}$) during each C-130 flight.

Flight #	$N_{50-400}/\text{cm}^{-3}$	$N_{>50}/\text{cm}^{-3}$
C-130 flight 6	-359 (-12)	-245 (-8)
C-130 flight 7	-231 (-7)	-213 (-6)
C-130 flight 8	+1 (+0.04)	+3 (+0.1)

to CCN we assume that all dust particles contain enough sulfate to make them active CCN. We find that dust leads to a decrease in N_{50-400} of 359 cm^{-3} (12%) and 231 cm^{-3} (7%) in flights 6 and 7, respectively. The addition of dust at sizes larger than 400 nm fails to compensate for the decrease in CCN below 400 nm. $N_{>50}$ decreases by 245 cm^{-3} (8%) and 213 cm^{-3} (6%) in flights 6 and 7. There are negligible changes in $N_{>50}$ and N_{50-400} in flight 8. So we conclude that the dust storm reduced the concentration of CCN-sized particles by up to 8%, even if all the dust particles simulated over the Yellow Sea contained enough soluble material to directly contribute to CCN.

5.2.2 Regional impacts on CCN-sized particles

Average modeled concentrations of CCN-sized particles during the dust storm period are presented in Fig. 10a and c. The model predicts N_{50-400} and $N_{>50}$ concentrations in excess of 4000 cm^{-3} across E. China, Korea and Japan. Throughout the Yellow Sea and Sea of Japan simulated concentrations are typically in excess of 2000 cm^{-3} .

Figure 10b shows that the inclusion of dust leads to a decrease in modeled boundary layer N_{50-400} by up to 10% across N. China and Mongolia, by <2% across most of E. China and the Sea of Japan, and by 2–5% over the Yellow Sea. Figure 10d shows that dust has the largest effect on $N_{>50}$ (>100%) across N. China and Mongolia. However, close to the source it is likely that the majority of these particles would be insoluble and therefore not active as CCN. In contrast, across E. China and the Yellow Sea dust particles make less than a 1% contribution to $N_{>50}$, so do not compensate for the decrease in N_{50-400} caused by the interaction of existing aerosol with dust.

6 Conclusions

The GLOMAP-bin model of aerosol microphysics has been used together with observations from the ACE-Asia experiment to examine dust-sulfate interactions during a large dust storm. Size resolved measurements of aerosol number and mass were obtained on the C-130 aircraft, providing detailed information on the characteristics of sulfate present in

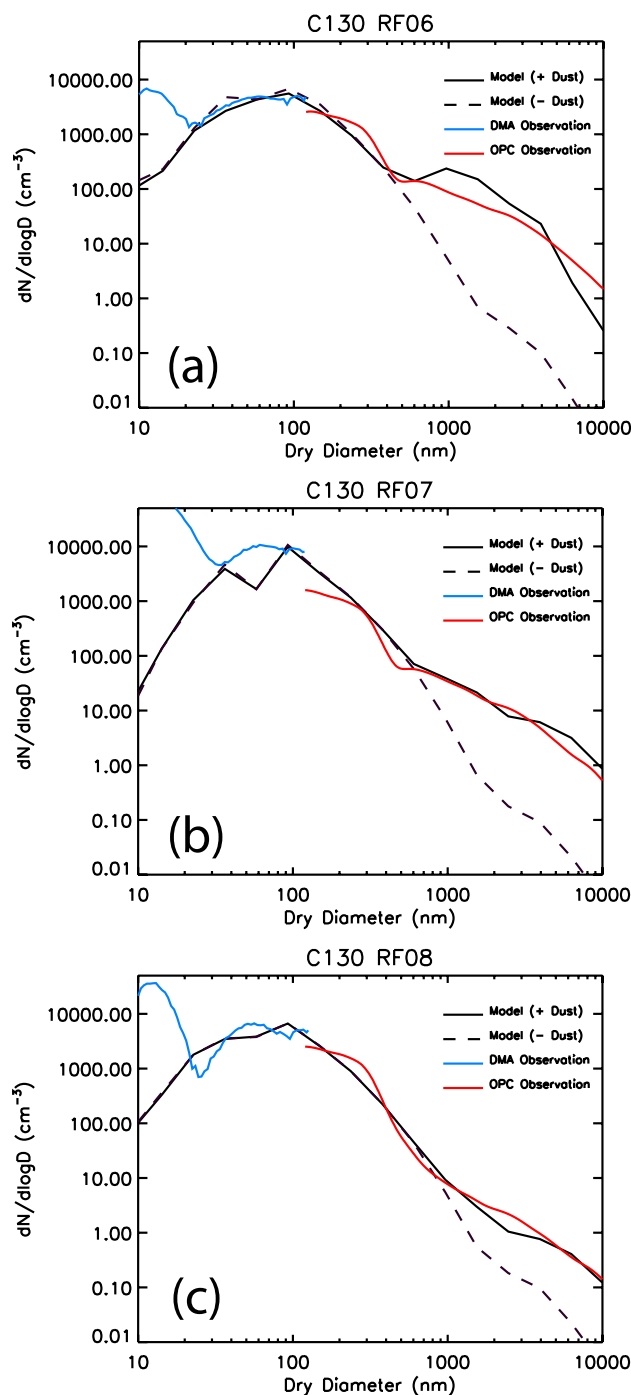


Fig. 9. Mean particle size distributions observed and modeled for flights (a) 6, (b) 7 and (c) 8 over periods when the dust concentration exceeded $100\text{ }\mu\text{g m}^{-3}$. Observations from the DMA (blue dashed) and OPC (red dashed) instruments are shown together with model results obtained from the DUST (black solid) and NODUST (black dashed) simulations.

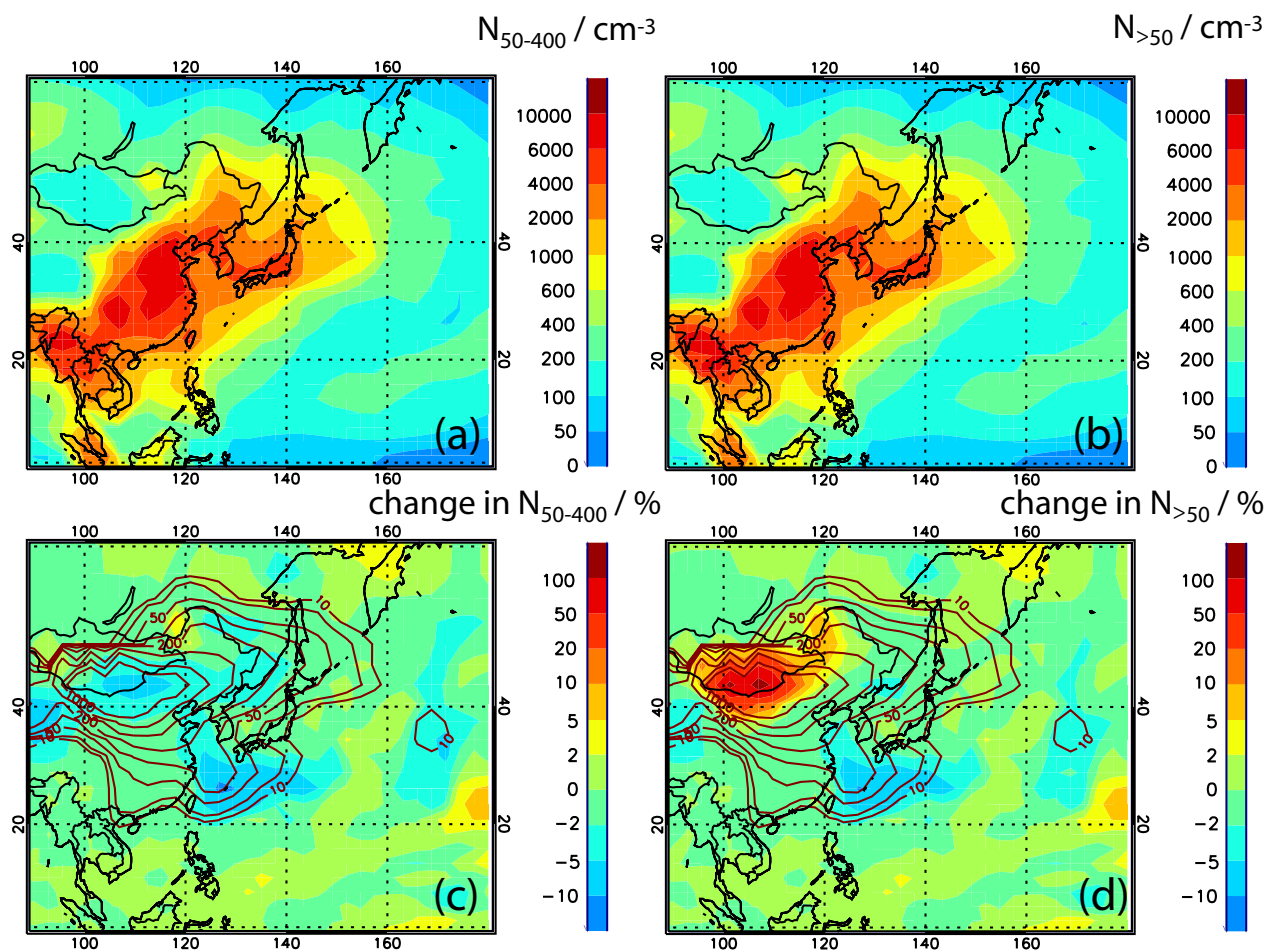


Fig. 10. Mean boundary layer (<1 km) particle concentrations at typical CCN sizes modeled in the dust storm period (6–14 April) for the NODUST simulation. (a) 50–400 nm diameter particle concentration (N_{50-400}), (b) 50–50 000 nm diameter particle concentration ($N_{>50}$), (c) percentage change in N_{50-400} following the inclusion of dust, (d) percentage change in $N_{>50}$ following the inclusion of dust. Brown isopleths show the mean boundary layer dust concentration ($\mu\text{g m}^{-3}$) over the same period.

dust-laden air. Although many previous model studies have attempted to quantify sulfate production on dust, few have examined how dust modifies the size of sulfate particles and little is known about how dust influences pre-existing aerosol number concentrations.

Model results were evaluated against observations from C-130 flights 6, 7 and 8 of the ACE-Asia campaign, during periods when modeled dust concentrations were predicted within a factor of 2 of observations. Approximately 60–90% of fine ($D_p < 1.3 \mu\text{m}$) sulfate mass concentrations are predicted within a factor of 2 of observations from the PILS instrument. We find that the net effect of dust is to reduce fine sulfate mass concentrations by less than 10%. This net reduction is made up of a decrease in sulfate below $0.4 \mu\text{m}$ by up to 45%, where the particles are mostly pure sulfate, and an increase from 0.4 – $1.3 \mu\text{m}$ of up to an order of magnitude due to sulfate associated with dust. The modeled sulfate concentration on fine dust is consistent with observations of the fraction of fine

sulfate associated with fine calcium (Maxwell-Meier et al., 2004). There were few observations of coarse ($D_p > 1.0 \mu\text{m}$) sulfate during each flight, but the model simulates 75% of the concentrations within a factor of 2 throughout flights 6, 7 and 8. Coarse sulfate is underpredicted by more than a factor of 10 when we exclude dust. These results suggest that dust was important for controlling the coarse sulfate concentrations observed by the C-130-aircraft and imply that GLOMAP-bin provides a reliable prediction of the rate at which sulfate was produced on coarse dust particles.

The fraction of sulfate observed and modeled at coarse sizes reached a maximum of 10–30% during the dust event over the Yellow Sea and Sea of Japan. However, the total sulfate inside the dust cloud increased by less than 2% because decreases in fine sulfate essentially compensated increases in coarse sulfate. Previous model studies have suggested that dust could increase the local sulfate mass burden by 10–100% downwind of E. Asia (Bauer and Koch, 2005;

Dentener et al., 1996; Song and Carmichael, 2001; Xiao et al., 1997). These studies also predicted that up to 70% of sulfate was present at coarse sizes over the Yellow Sea and Sea of Japan, at dust concentrations over an order of magnitude lower than observed in ACE-Asia. It would be reasonable to assume that if they had modeled sulfate formation onto this larger dust surface, they would have significantly overestimated the sulfate fractions observed on dust. Previous models may have overpredicted sulfate formation on dust by neglecting surface saturation effects for SO₂ on the dust surface. In contrast to these previous studies, we limit the amount of SO₂ oxidation on dust to a monolayer, and find that the uptake of H₂SO₄ can explain the sulfate present on dust in the ACE-Asia observations. If uptake of SO₂ onto dust were stronger in our model, we would overpredict coarse sulfate and significantly underestimate the SO₂ concentrations observed by the C-130 aircraft. Our findings support the conclusions of Song et al. (2007), who analyzed the composition of dust sampled in ACE-Asia C-130 flights 6, 7 and 8. They found that only a small fraction of mineral dust carbonate was displaced by acidic species, while previous model studies had predicted that carbonate would be strongly depleted in E. Asian outflow as a result of rapid accumulation of sulfate on the dust surface following heterogeneous oxidation of SO₂.

Dust impacts on the aerosol particle number concentration and size distribution observed over the ACE-Asia campaign have been studied here for the first time. GLOMAP-bin predicts up to 17% depletion in the particle concentration sampled during the dust storm. However, we find that dust has very little influence on aerosol that would make the most important contribution to CCN number (>50 nm dry diameter). The model predicts that CCN-sized particles were depleted by an average of less than 5% during an extreme dust event over E. China, Korea and Japan. This small decrease in existing CCN-sized particles is not compensated by the contribution from aged partly hygroscopic dust particles.

Acknowledgements. We acknowledge data provided by NCAR/EOL under sponsorship of the National Science Foundation (<http://data.eol.ucar.edu/>). GWM received funding from the UK National Centre for Atmospheric Science (NCAS). PTM was funded by an NCAS studentship. DVS was funded by the APPRAISE programme funded by NERC.

Edited by: Y. Balkanski

References

- Adams, J. W., Rodriguez, D., and Cox, R. A.: The uptake of SO₂ on Saharan dust: a flow tube study, *Atmos. Chem. Phys.*, 5, 2679–2689, 2005, <http://www.atmos-chem-phys.net/5/2679/2005/>.
- Alfaro, S. C. and Gomes, L.: Modeling mineral aerosol production by wind erosion: Emission intensities and aerosol size distributions in source areas, *J. Geophys. Res.*, 106(D16), 18075–18084, 2001.
- Alfaro, S. C., Gaudichet, A., Gomes, L., and Maille, M.: Mineral aerosol production by wind erosion: aerosol particle sizes and binding energies, *Geophys. Res. Lett.*, 25, 991–994, 1998.
- Andres, R. and Kasgnoc, A.: A time averaged inventory of subaerial volcanic sulfur emissions, *J. Geophys. Res.*, 103(D19), 25251–25262, 1998.
- Bates, T. S., Quinn, P. K., Coffman, D. J., Covert, D. S., and Miller, T. L.: Marine boundary layer dust and pollutant transport associated with the passage of a frontal system over eastern Asia, *J. Geophys. Res.*, 109, D19S19, doi:10.1029/2003JD004094, 2004.
- Bauer, S. E. and Koch, D.: Impact of heterogeneous sulfate formation at mineral dust surfaces on aerosol loads and radiative forcing in the Goddard Institute for Space Studies general circulation model, *J. Geophys. Res.*, 110, D17202, doi:10.1029/2005JD005870, 2005.
- Bond, T., Streets, D., Yarber, K. F., Nelson, K. S., Wo, J. H., and Klimont, Z.: A technology-based global inventory of black and organic carbon emissions from combustion, *J. Geophys. Res.*, 109, D14203, doi:10.1029/2003JD003697, 2004.
- Chun, Y., Kim, J., Choi, J. C., Boo, K. O., Oh, S. N., and Lee, M.: Characteristic number size distribution of aerosol during Asian dust period in Korea, *Atmos. Environ.*, 35, 2715–2721, 2001.
- Clarke, A. D., Shinozuka, Y., Kapustin, V. N., et al.: Size distributions and mixtures of dust and black carbon aerosol in Asian outflow: Physiochemistry and optical properties, *J. Geophys. Res.*, 109, D15S09, doi:10.1029/2003JD004378, 2004.
- Cofala, J., Amann, M., Klimont, Z., and Shopp, W.: Scenarios of world anthropogenic emissions of SO₂, NO_x, and CO up to 2030, Internal Report of the Transboundary Air Pollution Programme, International Institute for Applied Systems Analysis, Laxenburg, Austria, 2005.
- Dentener, F. J., Carmichael, G. R., Zhang, Y., Lelieveld, J., and Crutzen, P. J.: Role of mineral aerosol as a reactive surface in the global troposphere, *J. Geophys. Res.*, 101(D17), 22869–22890, 1996.
- Gong, S.: A parameterization of sea-salt aerosol source function for sub and super-micron particles, *Global Biogeochem. Cy.*, 17, 1097–1103, 2003.
- Goodman, A. L., Li, P., Usher, C. R., and Grassian, V. H.: Heterogeneous uptake of sulfur dioxide on aluminum and magnesium oxide particles, *J. Phys. Chem. A*, 105, 6109–6120, 2001.
- Grini, A., Zender, C. S., and Colarco, P. R.: Saltation Sandblasting behavior during mineral dust aerosol production, *Geophys. Res. Lett.*, 29, 1868, doi:10.1029/2002GL015248, 2002.
- Halmer, M., Schmincke, H., and Graf, H.: The annual volcanic gas input into the atmosphere, in particular into the stratosphere, A global data-set for the past 100 years, *J. Volcanol. Geoth. Res.*, 115, 511–528, 2002.

- Huebert, B. J., Bates, T., Russell, P. B., Shi, G., Kim, Y. J., Kawamura, K., Carmichael, G., and Nakajima, T.: An overview of ACE-Asia: Strategies for quantifying the relationships between Asian aerosols and their climatic impacts, *J. Geophys. Res.*, 108, 8633, doi:10.1029/2003JD003550, 2003.
- Jickells, T. D., An, Z. S., Andersen, K. K., et al.: Global iron connections between desert dust, ocean biogeochemistry, and climate, *Science*, 308, 67–71, 2005.
- Kettle, A. J. and Andreae, M. O.: Flux of dimethylsulfide from the oceans: A comparison of updated data sets and flux models, *J. Geophys. Res.*, 105, 26793–26808, 2000.
- Kline, J., Huebert, B., Howell, S., Blomquist, B., et al.: Aerosol composition and size versus altitude measured from the C-130 during ACE-Asia, *J. Geophys. Res.*, 109, D19S08, doi:10.1029/2004JD004540, 2004.
- Kulmala, M., Laaksonen, A., and Pirjola, L.: Parameterization for sulfuric acid/water nucleation rates, *J. Geophys. Res.*, 108(D7), 8301–8307, 1998.
- Lee, Y. H., Chen, K., and Adams, P. J.: Development of a global model of mineral dust aerosol microphysics, *Atmos. Chem. Phys.*, 9, 2441–2458, 2009, <http://www.atmos-chem-phys.net/9/2441/2009/>.
- Li, L., Chen, Z. M., Zhang, Y. H., Zhu, T., Li, J. L., and Ding, J.: Kinetics and mechanism of heterogeneous oxidation of sulfur dioxide by ozone on surface of calcium carbonate, *Atmos. Chem. Phys.*, 6, 2453–2464, 2006, <http://www.atmos-chem-phys.net/6/2453/2006/>.
- Liu, X., Penner, J., and Herzog, M.: Global modelling of aerosol dynamics: Model description, evaluation, and interactions between sulfate and nonsulfate aerosols, *J. Geophys. Res.*, 110, D18206, doi:10.1029/2004JD005674, 2005.
- Lunt, D. J. and Valdes, P. J.: The modern dust cycle: Comparison of model results with observations and study of sensitivities, *J. Geophys. Res.*, 107, 4669, doi:10.1029/2002JD002316, 2002.
- Manktelow, P. T., Mann, G. W., Carslaw, K. S., Spracklen, D. V., and Chipperfield, M. P.: Regional and global trends in sulfate since the 1980s, *Geophys. Res. Lett.*, 34, L14803, doi:10.1029/2006GL028668, 2007.
- Matsuki, A., Iwasaka, Y., Shi, G.-Y., et al.: Heterogeneous sulfate formation on the dust surface and its dependency on the mineralogy: Observational insight from the balloon-borne measurements in the surface atmosphere of Beijing, China, *Water Air Soil Pollut. Focus*, 5(3–6), 101–132, 2005a.
- Matsuki, A., Iwasaka, Y., Shi, G., Zhang, D., et al.: Morphological and chemical modification of mineral dust: Observational insight into the heterogeneous uptake of acidic gases, *Geophys. Res. Lett.*, 32, L22806, doi:10.1029/2005GL024176, 2005b.
- Maxwell-Meier, K., Weber, R., Song, C., Orsini, D., et al.: Inorganic composition of fine particles in mixed mineral dust – pollution plumes observed from airborne measurements during ACE-Asia, *J. Geophys. Res.*, 109, D19S07, doi:10.1029/2003JD004464, 2004.
- McNaughton, C. S., Clarke, A. D., Howell, S. J., Moore II, K. G., and Brekhovskikh, V.: Spatial distribution and size evolution of particles in Asian outflow: Significance of primary and secondary aerosols during ACE-Asia and TRACE-P, *J. Geophys. Res.*, 109, D19S06, doi:10.1029/2003JD003528, 2004.
- Meskhidze, N., Chameides, W. L., Nenes, A., and Chen, G.: Iron mobilization in mineral dust: Can anthropogenic SO₂ emissions affect ocean productivity?, *Geophys. Res. Lett.*, 30(21), 2085, doi:10.1029/2003GL018035, 2003.
- Meskhidze, N., Chameides, W. L., and Nenes, A.: Dust and pollution: A recipe for enhanced ocean fertilisation?, *J. Geophys. Res.*, 110, D03301, doi:10.1029/2004JD005082, 2005.
- Middleton, N. J.: A geography of dust storms in south-west Asia, *J. Climatol.*, 6, 183–196, 1986.
- Mori, I., Nishikawa, M., Tanimura, T., and Quan, H.: Change in size distribution and chemical composition of kosa (Asian dust) aerosol during long-range transport, *Atmos. Environ.*, 30, 4253–4263, 2003.
- Nightingale, P. D., Malin, G., Law, C. S., Watson, A. J., et al.: In situ evaluation of air-sea gas exchange parameterizations using novel conservative and volatile tracers, *Global Biogeochem. Cy.*, 14(1), 373–388, 2000.
- Ooki, A. and Uematsu, M.: Chemical interactions between mineral dust particles and acid gases during Asian dust events, *J. Geophys. Res.*, 110, D03201, doi:10.1029/2004JD004737, 2005.
- Perry, K. D., Cliff, S. S., and Jimenez-Cruz, M. P.: Evidence for hygroscopic mineral dust particles from the Intercontinental Transport and Chemical Transformation Experiment, *J. Geophys. Res.*, 109, D23S28, doi:10.1029/2004JD004979, 2004.
- Pozzoli, L., Bey, I., Rast, S., Schultz, M. G., Stier, P., and Feichter, J.: Trace gas and aerosol interactions in the fully coupled model of aerosol-chemistry-climate ECHAM5-HAMMOZ: 2. Impact of heterogeneous chemistry on the global aerosol distributions, *J. Geophys. Res.*, 113, D07309, doi:10.1029/2007JD009008, 2008.
- Prince, A. P., Kleiber, P., Grassian, V. H., and Young, M. A.: Heterogeneous interactions of calcite aerosol with sulfur dioxide and sulfur dioxide-nitric acid mixtures, *Phys. Chem. Chem. Phys.*, 9, 3432–3439, 2007.
- Satake, S., Uno, I., Takemura, T., Carmichael, G., and Tang, Y.: Characteristics of Asian aerosol transport simulated with a regional-scale chemical transport model during the ACE-Asia observation, *J. Geophys. Res.*, 109, D19S22, doi:10.1029/2003JD003997, 2004.
- Seinfeld, J. H., Carmichael, G. R., Arimoto, R., Conant, W. C., and Brechtel, F. J.: ACE-Asia regional climatic and atmospheric chemical effects of Asian dust and pollution, *B. Am. Meteorol. Soc.*, 85(2), 367–380, 2004.
- Song, C. H., Kim, C. M., Lee, Y. J., Carmichael, G. R., Lee, B. K., and Lee, D. S.: An evaluation of reaction probabilities of sulfate and nitrate precursors onto East Asian dust particles, *J. Geophys. Res.*, 112, D18206, doi:10.1029/2006JD008092, 2007.
- Song, C. H. and Carmichael, G. R.: A three-dimensional modeling investigation of the evolution processes of dust and sea-salt particles in east Asia, *J. Geophys. Res.*, 106(D16), 18131–18154, 2001.
- Spracklen, D. V., Pringle, K. J., Carslaw, K. S., Chipperfield, M. P., and Mann, G. W.: A global off-line model of size-resolved aerosol microphysics: I. Model development and prediction of aerosol properties, *Atmos. Chem. Phys.*, 5, 2227–2252, 2005, <http://www.atmos-chem-phys.net/5/2227/2005/>.

- Spracklen, D. V., Pringle, K. J., Carslaw, K. S., Chipperfield, M. P., and Mann, G. W.: A global off-line model of size-resolved aerosol microphysics: II. Identification of key uncertainties, *Atmos. Chem. Phys.*, 5, 3233–3250, 2005, <http://www.atmos-chem-phys.net/5/3233/2005/>.
- Spracklen, D. V., Pringle, K. J., Carslaw, K. S., Mann, G. W., Manktelow, P., and Heintzenberg, J.: Evaluation of a global aerosol microphysics model against size-resolved particle statistics in the marine atmosphere, *Atmos. Chem. Phys.*, 7, 2073–2090, 2007, <http://www.atmos-chem-phys.net/7/2073/2007/>.
- Stier, P., Feichter, J., Kinne, S., Kloster, S., Vignati, E., Wilson, J., Ganzeveld, L., Tegen, I., Werner, M., Balkanski, Y., Schulz, M., Boucher, O., Minikin, A., and Petzold, A.: The aerosol-climate model ECHAM5-HAM, *Atmos. Chem. Phys.*, 5, 1125–1156, 2005, <http://www.atmos-chem-phys.net/5/1125/2005/>.
- Sullivan, R. C., Guazzotti, S. A., Sodeman, D. A., and Prather, K. A.: Direct observations of the atmospheric processing of Asian mineral dust, *Atmos. Chem. Phys.*, 7, 1213–1236, 2007, <http://www.atmos-chem-phys.net/7/1213/2007/>.
- Tang, Y., Carmichael, G. R., Kurata, G., Uno, I., and Weber, R. J.: Impacts of dust on regional tropospheric chemistry during the ACE-Asia experiment: A model study with observations, *J. Geophys. Res.*, 109, D19S21, doi:10.1029/2003JD003806, 2004a.
- Tang, Y., Carmichael, G. R., Seinfeld, J. H., Dabdub, D., and Weber, R. J.: Three dimensional simulations of inorganic aerosol distributions in east Asia during spring 2001, *J. Geophys. Res.*, 109, D19S23, doi:10.1029/2003JD004201, 2004b.
- Taylor, K. E.: Summarizing multiple aspects of model performance in a single diagram, *J. Geophys. Res.*, 106(D7), 7183–7192, 2001.
- Tegen, I., Harrison, S. P., Kohfeld, K., Prentice, I. C., Coe, M., and Heinmann, M.: Impact of vegetation and preferential source areas on global dust aerosol: Results from a model study, *J. Geophys. Res.*, 107, 4576, doi:10.1029/2001JD000963, 2002.
- Trochkin, D., Iwasaka, Y., Matsuki, A., Yamanda, M., et al.: Mineral aerosol particles collected in Dunhuang, China, and their comparison with chemically modified particles collected over Japan, *J. Geophys. Res.*, 108, 8642, doi:10.1029/2002JD003268, 2003.
- Ullerstam, M., Vogt, R., Langer, S., and Ljungstrom, E.: The kinetics and mechanism of SO₂ oxidation by O₃ on mineral dust, *Phys. Chem. Chem. Phys.*, 4, 4694–4699, 2002.
- Ullerstam, M., Johnson, M. S., Vogt, R., and Ljungström, E.: DRIFTS and Knudsen cell study of the heterogeneous reactivity of SO₂ and NO₂ on mineral dust, *Atmos. Chem. Phys.*, 3, 2043–2051, 2003, <http://www.atmos-chem-phys.net/3/2043/2003/>.
- Uno, I., Satake, S., Carmichael, G. R., Tang, Y., and Wang, Z.: Regional chemical weather forecasting system CFORS: Model descriptions and analysis of surface observations at Japanese island stations during the ACE-Asia experiment, *J. Geophys. Res.*, 103, 8668, doi:10.1029/2002JD002845, 2003.
- Usher, C. R., Al-Hosney, H., Carlos-Cuellar, S., and Grassian, V. H.: A laboratory study of the heterogeneous uptake and oxidation of sulfur dioxide on mineral dust particles, *J. Geophys. Res.*, 107, 4713, doi:10.1029/2002JD002051, 2002.
- Van Curen, R. A. and Cahill, T. A.: Asian aerosols in North America: Frequency and concentration of fine dust, *J. Geophys. Res.*, 107(D24), 4804, doi:10.1029/2002JD002204, 2002.
- Van der Werf, G. R., Randerson, J. T., Collatz, G. J., and Giglio, L.: Carbon emissions from fires in tropical and subtropical ecosystems, *Global Change Biol.*, 9, 547–562, 2003.
- Watanabe, K., Kasuga, H., Yamada, Y., and Kawakami, T.: Size distributions of aerosol number concentrations and water-soluble constituents in Toyama, Japan: A comparison of the measurements during Asian dust period with non-dust period, *Atmos. Res.*, 82, 719–727, 2006.
- White, B. R.: Soil transport by winds on Mars, *J. Geophys. Res.*, 84, 4643–4651, 1979.
- Woodward, S.: Modelling the atmospheric life cycle and radiative impact of mineral dust in the Hadley Centre climate model, *J. Geophys. Res.*, 106(D16), 18155–18166, 2001.
- Xiao, H., Carmichael, G. R., Durchenwald, D., Thrornton, J., and Bandy, A.: Long-range transport of SO_x and dust in East Asia during the PEM B Experiment, *J. Geophys. Res.*, 102(D23), 28589–28612, 1997.
- Zakey, A. S., Solmon, F., and Giorgi, F.: Implementation and testing of a desert dust module in a regional climate model, *Atmos. Chem. Phys.*, 6, 4687–4704, 2006, <http://www.atmos-chem-phys.net/6/4687/2006/>.
- Zhao, T. L., Gong, S. L., Zhang, X. Y., and Jaffe, D. A.: Asian dust storm influence on North American ambient PM levels: observational evidence and controlling factors, *Atmos. Chem. Phys.*, 8, 2717–2728, 2008, <http://www.atmos-chem-phys.net/8/2717/2008/>.
- Zhang, D. Z., Shi, G. Y., Iwasaka, Y., and Hu, M.: Mixture of sulfate and nitrate in coastal atmospheric aerosols: individual particle studies in Qingdao (36 degrees 040 N, 120 degrees 210 E), China, *Atmos. Environ.*, 34, 2669–2679, 2000.
- Zobler, L.: A world soil file for global climate modelling, NASA Tech. Memo, 87802, 33 pp., 1986.